Optics Letters

Scattering of a cross-polarized linear wave by a soliton at an optical event horizon in a birefringent nanophotonic waveguide

CHARLES CIRET* AND SIMON-PIERRE GORZA

OPERA-Photonique, Université libre de Bruxelles (ULB), 50 av. F.D. Roosevelt, CP194/5, B-1050 Bruxelles, Belgium
**Corresponding author: charles.ciret@ulb.ac.be*

Received 24 March 2016; revised 13 May 2016; accepted 16 May 2016; posted 17 May 2016 (Doc. ID 261886); published 15 June 2016

The scattering of a linear wave on an optical event horizon, induced by a cross-polarized soliton, is experimentally and numerically investigated in integrated structures. The experiments are performed in a dispersion-engineered birefringent silicon nanophotonic waveguide. In stark contrast with copolarized waves, the large difference between the group velocity of the two cross-polarized waves enables a frequency conversion almost independent of the soliton wavelength. It is shown that the generated idler is only shifted by 10 nm around 1550 nm over a pump tuning range of 350 nm. Simulations using two coupled full vectorial nonlinear Schrödinger equations fully support the experimental results.

OCIS codes: (190.4380) Nonlinear optics, four-wave mixing; (190.5530) Pulse propagation and temporal solitons; (130.5440) Polarization-selective devices; (130.4310) Nonlinear.

http://dx.doi.org/10.1364/OL.41.002887

Nonlinear interactions between linear waves and solitons have attracted a tremendous amount of interest in the scientific community for many years. In this framework, interactions between waves of similar group velocities particularly draw the attention of researchers for their potential useful applications such as frequency converters [1] or for future optical transistor-like devices [2]. In this particular process, the propagation of an intense solitonic pump in a Kerr medium induces a moving refractive index perturbation, which in turn leads to a frequency conversion of a weak probe wave through a cross-phase modulation (XPM) process. In the context of supercontinuum (SC) generation, this process helps in understanding the underlying physics of the spectral broadening [3] and has also been demonstrated to enable the generation of highly coherent broadband SC [4,5] in a complementary manner to the well-known process involving the soliton fission [6–9]. This nonlinear interaction was originally elucidated as a four-wave mixing mechanism by Yulin and coworkers a decade ago [10,11]. Recently, it has been reinterpreted as the optical analog of the event horizon of black and white holes [12,13], as the intense pulse constitutes a horizon that light can neither join nor escape. These so-called optical event horizons have thus also largely been studied for their analogy with general relativity and in particular with the Hawking radiation [12].

Following its theoretical prediction, the experimental observation of such an effect has been realized in the context of SC generation in optical fibers [14]. Since then, numerous experimental and theoretical studies have been investigated, in various configurations [1,12,13,15–18]. Owing to the essential role played by the dispersion properties of the structure for the observation of an optical event horizon, almost all these demonstrations have been performed in photonic crystal fibers (PCFs), for which quasi on-demand dispersion properties can be engineered. Their observation in integrated structures has been reported only recently [19]. In this latter demonstration, the experiment was performed in silicon-on-insulator photonic wires which support optical soliton propagation [9,20]. The full complementary metal oxide semiconductor (CMOS) compatibility of silicon dispersion-engineered nanophotonic waveguides as well as the absence of a broad Raman gain could be very useful for applications.

Almost all of the previous studies have focused on the interaction between waves having the same polarization. Orthogonally polarized pump and probe waves have only been considered in the context of birefringent PCFs [14]. In this Letter, we report on the first experimental demonstration of the interaction that arises at the optical event horizon between two cross-polarized waves propagating in an integrated fully CMOS compatible birefringent nanophotonic waveguide. The dispersion properties of the two cross-polarized waves have been engineered through the waveguide dimensions, in order to allow for the two waves to interact. We show that the large difference between the group velocity dispersion of the two polarizations supported by our birefringent waveguide does not prevent the nonlinear interaction from occurring, provided that the proper phase matching condition is met. However, this phase matching condition is only weakly dependent on the pump wavelength for the waveguide considered in this work. As a result the wavelength of the generated idler wave is almost independent on the soliton wavelength. This is clearly different from the previously reported copolarized case. The ability to tailor the nonlinear interaction through the different dispersion

properties of the probe and the pump waves opens new possibilities, similarly to the works performed in the context of the sum frequency generation in thick type II nonlinear crystals [21]. The experimental results are fully supported by numerical simulations using two coupled full-vectorial generalized nonlinear Schrödinger equations.

When interacting in a Kerr medium, a pump and a probe waves with similar group velocities can lead to the generation of an idler wave set by the resonant condition [11,13,14,22]:

$$D(\omega_{\text{idler}} - \omega_{\text{pump}}) = D(\omega_{\text{probe}} - \omega_{\text{pump}}). \quad (1)$$

In this work, as two cross-polarized pump and probe waves are considered, $D(\omega - \omega_{\text{pump}})$ represents the wavenumber of a linear TM wave at a frequency ω in a reference frame comoving with the TE pump at a frequency ω_{pump}. The wavenumber D can be expressed as $D(\omega - \omega_{\text{pump}}) = \beta(\omega)_{\text{TM}} - \beta_{0_{\text{TE}}} - \beta_{1_{\text{TE}}} \times (\omega - \omega_{\text{pump}})$, where $\beta_{0_{\text{TE}}} = \beta(\omega_{\text{pump}})_{\text{TE}}$ and $\beta_{1_{\text{TE}}} = d\beta_{\text{TE}}/d\omega|_{\omega_{\text{pump}}}$. The wavelength dependence of the wavenumber D for the waveguide used in the experiments is displayed in Fig. 1 for two different (TE) pump wavelengths. In this figure, the velocity matched (VM) point is the wavelength of the TM mode that is group velocity matched with the TE pump wave. Considering a particular probe wavelength, the wavelength of the generated idler wave is located on the other side of the VM point, as depicted in Fig. 1. The wavelength conversion thus prevents the probe wave from crossing the pump pulse which constitutes its horizon.

Our demonstration is realized in a 6 mm long birefringent silicon-on-insulator nanophotonic waveguide, with a standard height of 220 nm and a width of 800 nm. This waveguide enables the propagation of both the fundamental quasi-TE and quasi-TM modes at wavelengths of interest, as confirmed by finite difference simulations performed using MODE Solutions from Lumerical. Because of the subwavelength dimensions of the structure and the high index contrast between the guiding and the surrounding regions, the two fundamental modes have non-negligible electric and magnetic longitudinal components [23]. These longitudinal components could lead to the coupling between the two polarizations during the propagation and modify the nonlinear coefficients usually encountered in the generalized scalar nonlinear Schrödinger equation. The set of two-coupled full vectorial nonlinear

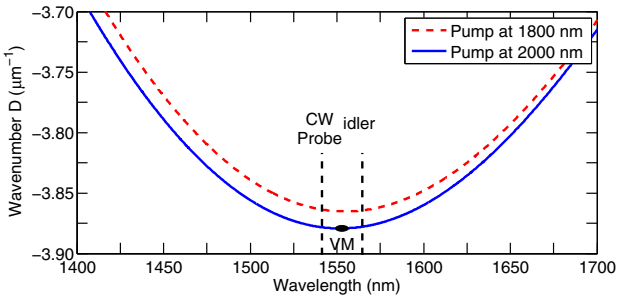

Fig. 1. Wavenumber D as a function of the wavelength for two pump wavelengths (birefringent case; see the text). The silicon nanophotonic waveguide under consideration is 220 nm thick and 800 nm wide. The two vertical dashed lines represent the position of a continuous probe wave (CW probe) at 1540 nm and the corresponding idler wavelength. VM point: group velocity-matched wavelength.

Schrödinger equations used to describe the propagation in our highly birefringent waveguide can be expressed as [23–25]

$$\frac{\partial a_\nu}{\partial z} = i\sum_{n=1}^{\infty}\frac{(i\partial/\partial t)^n}{n!}\beta_\nu^n a_\nu - \frac{\alpha_\nu}{2}a_\nu + (1+\tau_{\text{shock}}\partial/\partial t)[i\gamma_\nu|a_\nu|^2 a_\nu + 2i\gamma_{\mu\nu}|a_\mu|^2 a_\nu], \quad (2)$$

in which the subscripts $\nu, \mu = 1, 2$, with $\nu \neq \mu$, and $a_1(z,t)$, $a_2(z,t)$, denote the amplitudes of the quasi-TE and quasi-TM modes, respectively. In these equations, the coherent coupling terms between the polarization components have been neglected owing to the high birefringence of the waveguide. $\beta_\nu^n = \partial^n\beta_\nu/\partial\omega$ are the dispersion coefficients associated with the Taylor series expansion of the propagation constant of each mode $\beta_\nu(\omega)$ around the pump frequency ω_{pump}. These terms are responsible for the linear dispersion effect. In the simulations, as recommended by [6], the dispersion is, however, directly applied without any approximation in the frequency domain, from the function $\beta_\nu(\omega)$ evaluated for both polarizations using finite difference simulations. α_ν are the linear loss coefficients. They are assumed to be constant at 2 dB/cm for both polarizations on the wavelength range of interest. The dispersion of the nonlinearity is taken into account by the shock terms, as commonly used in previous studies [6,19]. Finally, $\gamma_\nu, \gamma_{\mu\nu}$ are the complex nonlinear parameters which are responsible for the self-modulation and the XPM effects, respectively. They are given by

$$\gamma_\nu = \frac{2\pi}{\lambda_\nu}\frac{\overline{n_{2_\nu}}}{A_{\text{eff}_\nu}} + i\frac{\overline{\beta_{\text{TPA}_\nu}}}{2A_{\text{eff}_\nu}},$$
$$\gamma_{\mu\nu} = \frac{2\pi}{\lambda_\nu}\frac{\overline{n_{2_{\mu\nu}}}}{A_{\text{eff}_{\mu\nu}}} + i\frac{\overline{\beta_{\text{TPA}_{\mu\nu}}}}{2A_{\text{eff}_{\mu\nu}}}, \quad (3)$$

in which A_{eff_ν} and $A_{\text{eff}_{\mu\nu}}$ are the generalized effective mode area and the overlapping generalized mode area between the two modes, respectively. $\overline{n_{2_\nu}}$, $\overline{n_{2_{\mu\nu}}}$ and $\overline{\beta_{\text{TPA}_\nu}}$, $\overline{\beta_{\text{TPA}_{\mu\nu}}}$ are the effective nonlinear refractive indexes and the effective two-photon absorption coefficients, averaged over an inhomogeneous cross section weighted with respect to the field distributions [23–25]. In Table 1, the value of the nonlinear parameters and of the generalized effective areas for both polarizations as well as the overlapping generalized effective area are given at the pump (TE) and the CW probe (TM) wavelengths. They have been estimated by calculating the electric and magnetic components of the mode profiles with finite difference simulations and from the values of the nonlinear indexes and the two-photon absorption coefficients reported in the literature [26]. Note that in Eq. (1), the free carrier dispersion and absorption as well as the Raman effect have been neglected, as they have a marginal impact on the nonlinear dynamics in our experimental conditions [19]. This

Table 1. Values of the Coefficients of Eq. (3), Corresponding to the Experiments

	TM-mode	TE-mode
λ (nm)	1540	2000
γ_ν ($\text{W}^{-1}\,\text{m}^{-1}$)	201 + 38i	220 + 18i
$\gamma_{\mu\nu}$ ($\text{W}^{-1}\,\text{m}^{-1}$)	66 + 7i	70 + 12i
A_{eff_ν} (μm^2)	0.324	0.205
$A_{\text{eff}_{\mu\nu}}$ (μm^2)	0.287	0.287

can simply be understood by the absence of a broad Raman gain close to the pump wavelength and by the low pulse energy and the carrier relaxation time (≈1 ns) which is much shorter than the delay between two pulses (12 ns). As shown in [19], the absence of the Raman soliton self-frequency shift is beneficial for potential applications of optical event horizons.

The experimental setup and the simulated dispersion curves for both polarizations are shown in Fig. 2. The nanowire possesses a low dispersion for the quasi-TE mode with a zero dispersion wavelength at 1700 nm, whereas for the TM mode the dispersion is always high and normal in the range 1400–1800 nm. Beyond this wavelength, the TM mode experiences a high linear loss. The input pump pulse is generated by an optical parametric oscillator delivering slightly chirped pulses (phase amplitude coupling factor $\alpha \approx 0.8$ [27]) with a duration of 200 fs full width at half-maximum at a wavelength of 2000 nm and with a 82 MHz repetition rate. Its polarization excites the fundamental quasi-TE mode of the structure. The CW probe is generated by a CW external cavity laser followed by an Er-doped fiber amplifier. Its wavelength can be tuned from 1525 to 1575 nm. At the amplifier output, the broad amplified spontaneous emission is filtered out by a tunable bandpass filter. The two collimated beams are combined on a dichroic mirror and coupled into the waveguide by means of a microscope objective. The polarization of the CW probe can be carefully adjusted using a half-wave-plate and a Glan–Thompson polarizer in order to excite either the fundamental quasi-TE or quasi-TM modes of the nanowire. At the waveguide output, the light is collected by a lensed fiber, then passes through a narrow filter to attenuate the remaining CW probe for a better visualization of the spectral features close to that wavelength. The filtered spectrum is recorded by an optical spectrum analyzer sensitive in the range 700–1700 nm. The experimental output spectra are displayed in Fig. 3(a) for an on-chip peak pump power of 3 W and a 500 μW CW probe at 1540 nm. At such peak power, the propagation of the pump alone in the anomalous dispersion region leads to the generation of a soliton of order $N = 1.7$ (nonlinear length at the input: 1.5 mm). Only part of its pedestal can be seen in the spectrum as the black curve in Fig. 3(a). The spectrum of

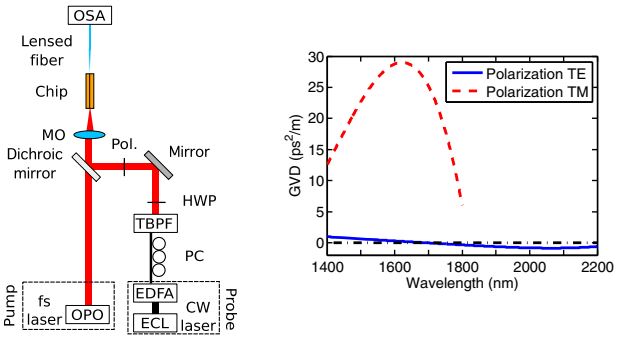

Fig. 2. Left: Experimental setup. OPO, optical parametric oscillator; ECL, external cavity laser; EDFA, erbium-doped fiber amplifier; PC, polarization controller; TBPF, tunable bandpass filter; HWP, half-wave-plate; Pol, polarizer; MO, microscope objective; Chip, silicon waveguide; OSA, optical spectrum analyzer. Right: Simulated group velocity dispersion curves for the TE-polarized (blue line curve) and the TM-polarized (red dashed curve) fundamental mode of the waveguide used in the experiments.

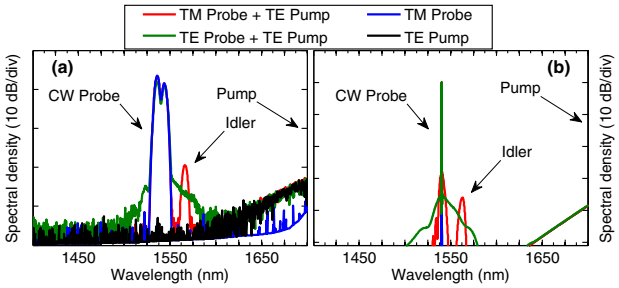

Fig. 3. (a) Experimental spectra recorded, with a 5 nm resolution, at the output of the 6 mm long Si waveguide and (b) the corresponding simulated spectra for the CW probe at 1540 nm and the pump at 2000 nm.

the TM-polarized CW probe alone is shown as the blue curve. When both the TM CW probe and the TE pump are propagating together, we can clearly observe the emergence of an idler wave at 1565 nm. This wavelength is in very good agreement with the phase matching condition, Eq. (1), represented as the blue curve in Fig. 1 for a pump wavelength of 2000 nm. When the polarization of the CW probe is rotated from TM to TE, only a wide pedestal close to the probe wavelength can be observed. This broadening is the result of the XPM induced on the CW probe by the soliton pulse. Further propagation shows the emergence of an idler wave as demonstrated in [19]. The simulations performed by solving the Eqs. (2) are plotted in Fig. 3(b). These results are in excellent agreement with the recorded experimental spectra. This confirms both the validity of the vectorial generalized nonlinear Schrödinger model, Eq. (2), and the interpretation of the experimental results. The higher efficiency of the frequency conversion when two cross-polarized waves are interacting can be explained by the dispersion properties of the two modes. As shown in [1], the conversion efficiency for a CW probe scales linearly with the group velocity difference between the probe and the soliton, and, in our waveguide, this difference is five times larger at 1540 nm for the TM probe than for the TE one.

The probe wave reflection on the optical event horizon is accompanied by a shift of its frequency leading to the appearance of the idler wave. This wavelength shift can be predicted on the basis of the phase-matching condition, Eq. (1), generalized for a cross-polarized interaction. It can simply be visualized in Fig. 1 as a reflection around the VM point. The wavelength dependence of the idler wave as a function of the probe wavelength is plotted in Fig. 4(a). The experimental results are in very good agreement with the simulations and with Eq. (1). As can be seen, as the probe wavelength is tuned closer to the VM point, the idler wavelength also gets closer to that particular wavelength. More interestingly, it is shown in Fig. 4(b) that for a fixed probe wavelength of 1540 nm, the idler wavelength is almost independent of the pump wavelength. As the pump wavelength is tuned from 1750 up to 2100 nm, the idler wavelength is only shifted by 10 nm. This can be explained from the very low group velocity dispersion coefficient of the quasi-TE mode compared to the quasi-TM mode. As a result of this large difference, the particular wavelength corresponding to the VM point around which the reflection of the probe on the optical event horizon occurs is only slightly shifted over a large pump wavelength range (see in Fig. 1). This behavior is not encountered for copolarized TE interactions as the dispersion

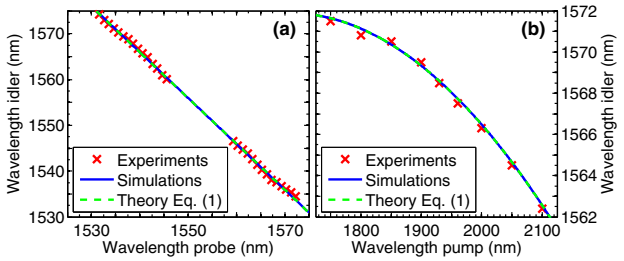

Fig. 4. (a) Wavelength of the idler wave as a function of the CW probe wavelength for a pump at 2000 nm. There are no experimental results in the range 1545–1555 nm because the wavelengths of the CW probe and the idler are too close to be distinguishable. (b) Evolution of the idler wavelength with the pump wavelength for a CW probe at 1540 nm. The pump power has been adjusted to avoid exciting a higher-order soliton.

coefficients are closer for the probe and the pump waves (see in Fig. 2). Finally, note that no spectral recoil of the pump, associated with the scattering of the probe, has been observed in the experimental or simulated spectra. This comes from the too low energy transfer, inherent to the scattering of the low CW wave, as shown in [19] for copolarized interactions. The simulations with a pulsed probe reveal however, that in this latter case, a spectral recoil of the pump is observable and is associated with a 70% energy conversion of the probe (not shown). For a pulsed probe at 1540 nm, the interaction takes place in 1.5 mm.

In conclusion, we have experimentally and numerically investigated the scattering of a cross polarized linear wave by a soliton at an optical event horizon in a birefringent nanophotonic waveguide. The simulations were performed by integrating a set of two coupled vectorial generalized nonlinear Schrödinger equations. In these equations, the longitudinal components of the electric and magnetic fields have been taken into account owing to the high index contrast subwavelength nanophotonic waveguides considered in this work. These components are responsible for the coupling between the two cross polarizations for low birefringent waveguides and change the expressions of the nonlinear coefficients. As the birefringence of our dispersion engineered waveguide is large, the longitudinal components have only been taken into account in the expression of the nonlinear coefficients. In the experiment, we have unambiguously observed the emergence of an idler wave when an intense quasi-TE pump pulse propagates together with a quasi-TM CW probe. The large difference in the group velocity dispersion coefficients for the two polarizations leads to a high net conversion efficiency as well as a low dependence with the pump wavelength on the generated idler wavelength, located in the C-band in this work. These results, very well supported by the numerical simulations, are in contrast with previously reported results and could be useful for potential integrated applications.

Funding. Belgian Science Policy Office (BELSPO); Interuniversity Attraction Poles Program Project Photonics (IAP 7-35); Fonds de la Recherche Fondamentale Collective (FRFC) (PDR.T.1084.15).

Acknowledgment. The authors thank B. Kuyken, G. Roelkens, U. D. Dave, and F. Leo for the fruitful discussions and for providing the Si waveguide.

REFERENCES

1. L. Tartara, IEEE J. Quantum Electron. **48**, 1439 (2012).
2. A. Demircan, S. Amiranashvili, and G. Steinmeyer, Phys. Rev. Lett. **106**, 163901 (2011).
3. D. V. Skryabin and A. V. Gorbach, Rev. Mod. Phys. **82**, 1287 (2010).
4. A. Demircan, S. Amiranashvili, C. Brée, and G. Steinmeyer, Phys. Rev. Lett. **110**, 233901 (2013).
5. A. Demircan, S. Amiranashvili, C. Brée, U. Morgner, and G. Steinmeyer, Opt. Express **22**, 3866 (2014).
6. J. M. Dudley, G. Genty, and S. Coen, Rev. Mod. Phys. **78**, 1135 (2006).
7. F. Leo, S.-P. Gorza, S. Coen, B. Kuyken, and G. Roelkens, Opt. Lett. **40**, 123 (2015).
8. U. D. Dave, C. Ciret, S.-P. Gorza, S. Combrie, A. D. Rossi, F. Raineri, G. Roelkens, and B. Kuyken, Opt. Lett. **40**, 3584 (2015).
9. W. Ding, C. Benton, A. V. Gorbach, W. J. Wadsworth, J. C. Knight, D. V. Skryabin, M. Gnan, M. Sorrel, and R. M. De La Rue, Opt. Express **16**, 3510 (2008).
10. A. V. Yulin, D. V. Skryabin, and P. St. J. Russell, Opt. Lett. **29**, 2411 (2004).
11. D. V. Skryabin and A. V. Yulin, Phys. Rev. E **72**, 016619 (2005).
12. T. G. Philbin, C. Kuklewicz, S. Robertson, S. Hill, F. König, and U. Leonhardt, Science **319**, 1367 (2008).
13. K. E. Webb, M. Erkintalo, Y. Xu, N. G. R. Broderick, J. M. Dudley, G. Genty, and S. G. Murdoch, Nat. Commun. **5**, 4969 (2014).
14. A. Efimov, A. V. Yulin, D. V. Skryabin, J. C. Knight, N. Joly, F. G. Omenetto, A. J. Taylor, and P. Russell, Phys. Rev. Lett. **95**, 213902 (2005).
15. S. F. Wang, A. Mussot, M. Conforti, A. Bendahmane, X. L. Zeng, and A. Kudlinski, Phys. Rev. A **92**, 023837 (2015).
16. S. F. Wang, A. Mussot, M. Conforti, X. L. Zeng, and A. Kudlinski, Opt. Lett. **40**, 3320 (2015).
17. A. V. Yulin, R. Driben, B. A. Malomed, and D. V. Skryabin, Opt. Express **21**, 14481 (2013).
18. I. Oreshnikov, R. Driben, and A. V. Yulin, Opt. Lett. **40**, 5554 (2015).
19. C. Ciret, F. Leo, B. Kuyken, G. Roelkens, and S.-P. Gorza, Opt. Express **24**, 114 (2016).
20. J. Zhang, Q. Lin, G. Piredda, R. W. Boyd, G. P. Agrawal, and P. M. Fauchet, Opt. Express **15**, 7682 (2007).
21. P. Wasylczyk, A. B. U'ren, P. J. Mosley, J. Lundeen, M. P. A. Branderhorst, S.-P. Gorza, A. Monmayrant, A. Radunsky, and I. A. Walmsley, J. Mod. Opt. **54**, 1939 (2007).
22. Y. Q. Xu, M. Erkintalo, G. Genty, and S. G. Murdoch, Opt. Lett. **38**, 142 (2013).
23. S. Afshar and T. M. Monro, Opt. Express **17**, 2298 (2009).
24. B. A. Daniel and G. P. Agrawal, J. Opt. Soc. Am. B **27**, 956 (2010).
25. S. Afshar, M. A. Lohe, W. Q. Zhang, and T. M. Monro, Opt. Express **20**, 14514 (2012).
26. A. D. Bristow, N. Rotenberg, and H. M. van Driel, Appl. Phys. Lett. **90**, 191104 (2007).
27. P. Lazaridis, G. Debarge, and P. Gallion, Opt. Lett. **20**, 1160 (1995).